# Dynamic properties of the energy loss of multi-MeV charged particles traveling in two-component warm dense plasmas

Zhen-Guo Fu,[1,2] Zhigang Wang,[2] Meng-Lei Li,[1,2] Da-Fang Li,[2] Wei Kang,[3,*] and Ping Zhang[1,2,3,4,†]

[1]*Center for Fusion Energy Science and Technology, CAEP, P.O. Box 8009, Beijing 100088, China*

[2]*Institute of Applied Physics and Computational Mathematics, P.O. Box 8009, Beijing 100088, China*

[3]*HEDPS, Center for Applied Physics and Technology, Peking University, Beijing 100871, China*

[4]*Center for Compression Science, CAEP, Mianyang 621900, China*

(Received 28 August 2016; published 9 December 2016)

The energy loss of multi-MeV charged particles moving in two-component warm dense plasmas (WDPs) is studied theoretically beyond the random-phase approximation. The short-range correlations between particles are taken into account via dynamic local field corrections (DLFC) in a Mermin dielectric function for two-component plasmas. The mean ionization states are obtained by employing the detailed configuration accounting model. The Yukawa-type effective potential is used to derive the DLFC. Numerically, the DLFC are obtained via self-consistent iterative operations. We find that the DLFC are significant around the maximum of the stopping power. Furthermore, by using the two-component extended Mermin dielectric function model including the DLFC, the energy loss of a proton with an initial energy of ∼15 MeV passing through a WDP of beryllium with an electronic density around the solid value $n_e \approx 3 \times 10^{23}$ cm$^{-3}$ and with temperature around ∼40 eV is estimated numerically. The numerical result is reasonably consistent with the experimental observations [A. B. Zylsta *et al.*, Phys. Rev. Lett. **111**, 215002 (2013)]. Our results show that the partial ionization and the dynamic properties should be of importance for the stopping of charged particles moving in the WDP.

DOI: 10.1103/PhysRevE.94.063203

## I. INTRODUCTION

To realize the ignition and high-energy gain in inertial confinement fusion (ICF), more and more efforts have been devoted to investigating the physical properties involved in the ICF [1–9]. The problem of the energy loss of protons and $\alpha$-particles produced via fusion reactions (such as $D + {}^3He \rightarrow \alpha + p$) in dense plasmas is of considerable significance for understanding and controlling the implosion dynamics to ensure successful ICF. Many theoretical models for the stopping power have been developed. The first classical theoretical model on this issue may have been proposed by Bohr [10], followed by Bethe using perturbative quantum-mechanical calculations [11]. Later, more elaborate approaches beyond the perturbation theory were also developed [12–25]. For instance, the dielectric function model under the random-phase approximation (RPA) [12,13] has been widely used to describe the stopping power of plasmas to charged particles. To take into account the effects of collisions, the RPA dielectric model has extended the Mermin dielectric model [15] via the relaxation-time approximation. Furthermore, an extension of the conventional Mermin model incorporating both static local-field corrections (SLFC) $G_{\alpha\beta}(k,\omega = 0)$ with $\alpha,\beta = e$ or $i$ [18] has been suggested in Ref. [22]. The influences of the electron-ion ($e$-$i$) dynamic collision frequency (DCF) and electron-electron ($e$-$e$) dynamic local field corrections (DLFC) on Thomson scattering in plasmas has been discussed via an extended one-component Mermin model [24]. Recently, the stopping power of hydrogenlike plasma has been studied via the moment method and the extended Mermin model, but local-field corrections were not introduced to the classical dielectric function of ions [25]. Molecular-dynamics simulations [26] have also been employed to simulate the classical charged-particle stopping power in weakly coupled deuterium-tritium (DT) plasmas. The simulations were compared with those obtained from Boltzmann and Lenard-Balescu kinetic equations [27] and fully convergent theories [19,21] to establish the validity of present models.

At present, ion stopping in cold matter is relatively well understood, with abundant experimental data [28] and several available simulation codes [29–31]. Nazarov *et al.* have also developed a rigorous formula for the stopping power of solids for slow ions. In their theoretical formula, the effects of dynamical correlation are included through the exchange-correlation kernel of time-dependent density-functional theory [32,33]. However, ion stopping in ionized plasmas is far from being understood because of various theoretical and experimental challenges. Only a few experimental data have been collected. Recently, the stopping of ions produced in the nuclear reactions in weakly coupled hot dense plasmas has been measured quantitatively on the OMEGA laser facility [34], and the experimental results generally support the predictions of the Brown-Preston-Singleton (BPS) [21] and Li-Petrasso (LP) models [19]. This experiment indicates that both the BPS model and the LP model are suitable for weakly coupled plasmas, in which the stopping power may be assumed as a summation of binary collisions. Another experiment on the stopping power of protons in a warm dense plasma (WDP) of beryllium (Be) with solid density and an electron temperature of $\sim 32 \pm 15$ eV [35] cannot be perfectly explained by the BPS model and the LP model. Dielectric response, in contrast, should be a good way to understand the properties of WDP, including the stopping power of WDP on the charged particles. This is because the WDP are strongly influenced by several

*weikang@pku.edu.cn

†zhang_ping@iapcm.ac.cn

 

physical properties (e.g., the effects of particle screening, electron degeneracy, and correlations between electrons and ions). Under the RPA and average-atom frames [16,17,20,23], the analysis in Ref. [35] indicated the importance of the partial ionization [36,37] and the bound-free electron transitions [38] for the stopping of charged particles in the WDP. Additionally, the dynamic characteristics [39–41], the strong correlation effect between component particles [42,43], as well as the unique transport properties [44,45] in the WDP are also very different from those in the weakly coupled hot dense plasmas. These unique physical properties will certainly give rise to remarkably different behaviors of the charged particles moving in the WDP.

The influences of DCF and DLFC on the charged-particle stopping in WDP of Be has not been considered in the current literature. However, the dynamic properties in this regime should also be remarkable for the stopping of particles. Due to the importance from the perspectives of both basis physics and potential applications of Be in the fields of ICF, it is interesting and timely to provide a theoretical analysis of the dynamic properties of energy loss of charged particles traveling in the WDP of Be. Therefore, from this aspect, we present in this paper a theoretical investigation on this problem based on the dielectric function models. The extended Mermin dielectric function (EMDF) model containing the DCF and DLFC may provide a reliable method applied to this issue.

The detailed configuration accounting model and the average-atom model are used to determine the mean ionization state, and the Yukawa-type effective potential is also employed. We find that the DLFC is significant around the maximum of the stopping power. Furthermore, by using the two-component EMDF, the energy loss of a proton with an initial energy of ∼15 MeV passing through a WDP of Be with an electronic density around the solid values $n_e \approx 3 \times 10^{23}$ cm$^{-3}$ and with temperature around ∼40 eV is estimated numerically. The numerical result is reasonably consistent with the experimental observations [35]. However, the theoretical stopping power under the RPA frame does not agree with the experimental data. Our results show that the partial ionization and the dynamic properties should be of importance for the stopping power of charged particles moving in the WDP.

The text is organized in the following fashion. In Sec. II we present the extended two-component Mermin dielectric function model for the stopping of charged particles in WDP. Section III contains a detailed investigation of the dynamic properties of the energy loss of a proton moving in the WDP. For comparison, the static results of the stopping power are also illustrated. Numerical results for the energy loss of a proton moving in a WDP of Be are also presented and discussed in this section. A brief summary and conclusions are given in Sec. IV.

## II. THEORETICAL MODEL DESCRIPTION

Based on the concept of relaxation time, one can easily get the Mermin dielectric function for degenerate electrons [15]. For degenerate plasma, the Fermi distribution function is used to get the dielectric function. In the classical limit, the Maxwell-Boltzmann statistics may be applied, and thus the Fermi distribution function will be replaced by the Maxwell-Boltzmann distribution function. Therefore, the Mermin dielectric function should still be valid for the classical ions. The generalization of the Mermin dielectric function to a multicomponent plasma is straightforward. One has to sum up the polarization functions of all components of the system [46–48]. Considering the mixing rule [46,47], the Mermin dielectric function of multicomponent plasmas is generalized into

$$\epsilon_M(k,\omega) = 1 + \sum_{\alpha=e,i} \frac{[\omega + i\nu_\alpha(\omega)]\{\epsilon_\alpha[k,\omega + i\nu_\alpha(\omega)] - 1\}}{\omega + i\nu_\alpha(\omega)\frac{\epsilon_\alpha[k,\omega+i\nu_\alpha(\omega)]-1}{\epsilon_\alpha(k,0)-1}}, \tag{1}$$

where $\nu_\alpha(\omega)$ is the DCF with $\nu_{\alpha=e}(\omega) \equiv \nu(\omega)$ for electrons and $\nu_{\alpha=i}(\omega) = (m_e/m_i)^{1/2}\nu(\omega) \equiv \nu'(\omega)$ for ions. Under the Born approximation scheme, the DCF $\nu(\omega)$ is expressed as

$$\nu(\omega) = \int_0^\infty dk\, U(k) \frac{\epsilon_e(k,\omega) - \epsilon_e(k,0)}{i\omega\omega_p^2}, \tag{2}$$

where $\omega_p = (n_e e^2/m_e)^{1/2}$ is the electron plasma frequency, and $U(k) = \frac{n_i}{6\pi^2 m_e^2} k^6 V_{ei}^2(k) S_{ii}(k)$, with $V_{ei}(q) = -\frac{4\pi\langle Z\rangle e^2}{k^2\epsilon_e(k,0)}$ being the screened *e-i* interaction potential and $S_{ii}(k)$ being the *i-i* static structure factor. Here, $\epsilon_\alpha(k,\omega)$ is the RPA dielectric function for the free plasma component $\alpha$.

Furthermore, these models may still be deficient in describing the WDP, whose densities are approximated as solid density and whose temperatures are around tens of eV. The reason is that the effects of particle screening, electron degeneracy, and correlations between electrons and ions in the WDP become of importance. These correlations can be described via the DLFC $G_{\alpha\beta}(k,\omega)$. The DLFC can be directly introduced in the RPA dielectric function in the following form (e.g., for electron plasma):

$$\tilde{\epsilon}_e(\boldsymbol{k},\omega) = 1 - \frac{1 - \epsilon_e(\boldsymbol{k},\omega)}{1 + [1 - \epsilon_e(\boldsymbol{k},\omega)]G_{ee}(k,\omega)}. \tag{3}$$

The expression for the dielectric function of ion plasmas, i.e., $\tilde{\epsilon}_i(\boldsymbol{k},\omega)$, is easily obtained by considering the DLFC $G_{ii}(k,\omega)$. Additionally, the EMDF $\tilde{\epsilon}_M(k,\omega)$ including the DLFC for multicomponent plasmas could be obtained by changing $\epsilon_\alpha(\boldsymbol{k},\omega)$ in Eq. (1) as $\tilde{\epsilon}_\alpha(\boldsymbol{k},\omega)$. We will not show the expression of $\tilde{\epsilon}_M(k,\omega)$ for the sake of brevity. The advantage of EMDF $\tilde{\epsilon}_M(k,\omega)$ is that it can be easily deduced into the static limit by taking $G_{\alpha\alpha}(k,\omega \to 0)$ and $\nu(\omega \to 0)$. It is also suitable for the plasmas, especially the WDP, at any degeneracy. Both static and dynamic results could be obtained self-consistently. Therefore, the EMDF model provides more accurate calculations for the observable quantities in experiments, such as the energy loss of charged particles moving in the plasmas.

Several approximative approaches to the DLFC have been proposed in the literature [18,22,24,39,49]. In this work, we employ the approach developed by Hong and Lee [49]. It advocates a smooth interpolation between the two SLFCs at $\omega = 0$ and $\omega = \infty$ presented by

$$G_{\alpha\alpha}(k,\omega) = G_{\alpha\alpha}(k,0) + [G_{\alpha\alpha}(k,\infty) - G_{\alpha\alpha}(k,0)]\mathcal{G}_\alpha(k,\omega), \tag{4}$$

where $\alpha = e,i$, and

$$\mathcal{G}_e(k,\omega) = \mathcal{G}_0(k)\frac{\epsilon_e(k,0)-\epsilon_e(k,\omega)}{\epsilon_e(k,\omega)-1} + \frac{\omega^2[1-\epsilon_e(k,0)]}{\omega_p^2}, \quad (5)$$

$$\mathcal{G}_i(k,\omega) = \mathcal{G}_0(k)\frac{\epsilon_i(k,0)-\epsilon_i(k,\omega)}{\epsilon_i(k,\omega)-1} + \frac{\omega^2\pi m_i}{k^2+\kappa_i^2}, \quad (6)$$

with $\mathcal{G}_0(k) = [\frac{\hbar^2k^4[1-\epsilon_e(k,0)]}{4m_e n_e e^2} - 1]^{-1}$ for free electrons while $\mathcal{G}_0(k) = \frac{1}{2}$ for classical ions. In our derivations, the Yukawa effective interaction potential [50–54] is used, and the explicit expressions for the SLFCs $G_{\alpha\alpha}(k,0)$ and $G_{\alpha\alpha}(k,\infty)$ are shown in Appendix B.

The stopping power for a pointlike ion with charge $Z_p$ and mass $m_p$ traveling with velocity $v_p$ through the plasmas is written as [55]

$$\frac{dE}{dx} = \frac{2Z_p^2e^2}{\pi v_p^2}\int_0^\infty \frac{dk}{k}\int_{\omega_-(k)}^{\omega_+(k)} d\omega\left(\omega - \frac{\hbar k^2}{2m_p}\right)\frac{\mathrm{Im}[\epsilon(k,\omega)]^{-1}}{e^{-\hbar\omega/T}-1}, \quad (7)$$

where $\omega_\pm(k) = \hbar k^2/2m_p \pm kv_p$. It is clear that the stopping power depends on the dielectric function of background plasmas. From this formula, one can compare the stopping power given by the different dielectric functions. Following the method in Ref. [55], a general formula of the stopping power based on the dielectric function theory could be obtained within any type of interaction potentials. Here, the screening effect is taken into account by the dielectric function presented in Eq. (7). In particular, in our calculations, the screening effect of the Yukawa potential is also included in the EMDF via the DLFC, which is a straightforward generalization of the model derived by using the Coulomb potential [56]. The Yukawa potential has been variously employed to study the collective excitations [52,53] and the stopping power of plasmas [57–61]. For instance, based on the Yukawa potential, an analytical dielectric function model for the energy loss of charged particles moving over a two-dimensional dusty plasma has been developed, and the theoretical results obtained from this model are well consistent with the molecular-dynamics simulations [59–61]. Our formula shown here may be applied to the stopping power of solids for slowly injected ions, since the correlation effects should be of importance in an interacting electron gas, which has been studied by using the time-dependent density-functional theory [32,33].

## III. RESULTS AND DISCUSSIONS

Before discussing the energy loss of a multi-MeV proton passing through a WDP of Be, let us first discuss the mean ionization degree of an average ion $\langle Z\rangle$ for Be. Numerical calculations based on two different models, namely a detailed configuration accounting model [37] and an average-atom model [36], have been performed. The effect of pressure ionization is considered in both models. The results show that the degree of ionization for Be based on these two models is almost identical. Typical results of the mean ionization degree $\langle Z\rangle$ for $\rho_{\mathrm{Be}} = 1.85$ g/cm$^3$ obtained by a detailed configuration accounting model are presented in Fig. 1(a). The mean ionization state is $\langle Z\rangle = 2$ when the temperature is less than 10 eV, and it is almost fully ionized ($\langle Z\rangle > 3.9$) when the temperature is greater than 800 eV. Correspondingly, the uniform number density of electrons $n_e$ is shown in Fig. 1(b). We find that the number density of electrons is $n_e \approx 2.5\times10^{23}$ cm$^{-3}$ when the temperature is less than 10 eV, and it increases gradually to $n_e \approx 4.8\times10^{23}$ cm$^{-3}$ when the temperature is increased to more than 800 eV. The electron chemical potential $\mu$ is obtained by the charge-neutrality condition that $\langle Z\rangle n_i = \frac{(2m_eT)^{3/2}}{2\pi^2\hbar^3}F_{1/2}(\mu)$, with $F_\delta(\eta) = \int_0^\infty \frac{x^\delta dx}{e^{(x-\eta)}+1}$ being the $\delta$th-order Fermi integral. The chemical potential gradually decreases with increasing temperature; see Fig. 1(c).

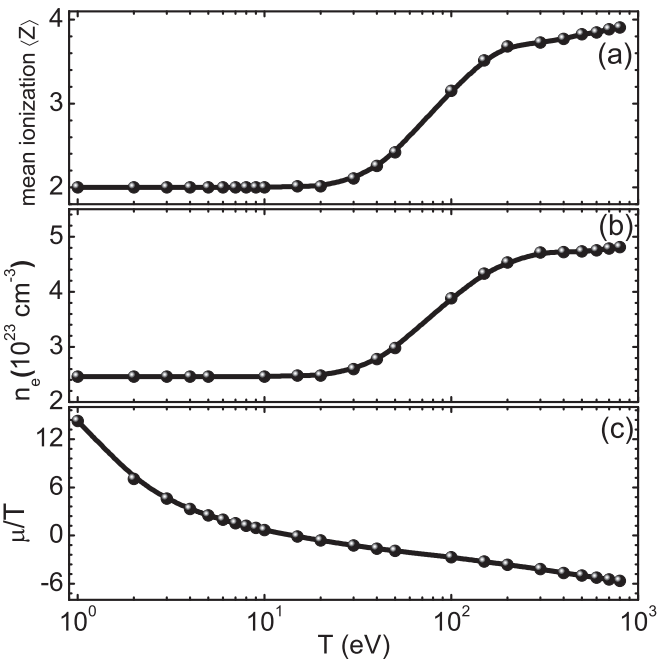


FIG. 1. (a) The mean ionization degree $\langle Z\rangle$ of an average ion, (b) the number densities of electrons, and (c) the chemical potential as a function of temperature of Be at solid density of $\rho_{\mathrm{Be}} = 1.85$ g/cm$^3$.

The results of DCF $\nu(\omega)$ as a function of the frequency $\omega$ are shown in Fig. 2. Figure 2(a) is for the WDP of Be with an electron number density $n_e = 10^{23}$ cm$^{-3}$ and three different temperatures $T = 1$, 10, and 100 eV, while Fig. 2(b) is for the WDP of Be with a temperature $T = 10$ eV and three different densities $n_e = 10^{23}$, $10^{24}$, and $10^{25}$ cm$^{-3}$. In Fig. 2, the solid curves denote the real part of DCF, and the dotted curves denote the imaginary part of DCF. In all the calculations, the mean ionization degree $\langle Z\rangle$ is considered via a detailed configuration accounting model. The DCF decreases with increasing both temperature and electron density.

The imaginary part of DCF Im $\nu(\omega)$ is connected to the real part of DCF Re $\nu(\omega)$ by a Kramers-Kronig relation so that Im $\nu(\omega) = \int_{-\infty}^{\infty}\frac{d\omega'}{\pi}\frac{\mathrm{Re}\,\nu(\omega')}{\omega-\omega'}$. The account of this imaginary part is essential for obeying both the $f$-sum rule and the perfect screening sum rule [25]. Loosely speaking, the real part of $\nu(\omega)$ leads to a broadening of the plasmon at $k = 0$, and the imaginary part produces a shift in the plasmon. In the high-frequency limit $\omega\to\infty$, the real part of $\nu(\omega)$ vanishes and the DCF is approximated as a pure imaginary quantity. The derivations of the high-frequency limit of DCF are shown in Appendix C. In the static limit $\omega\to0$, the imaginary

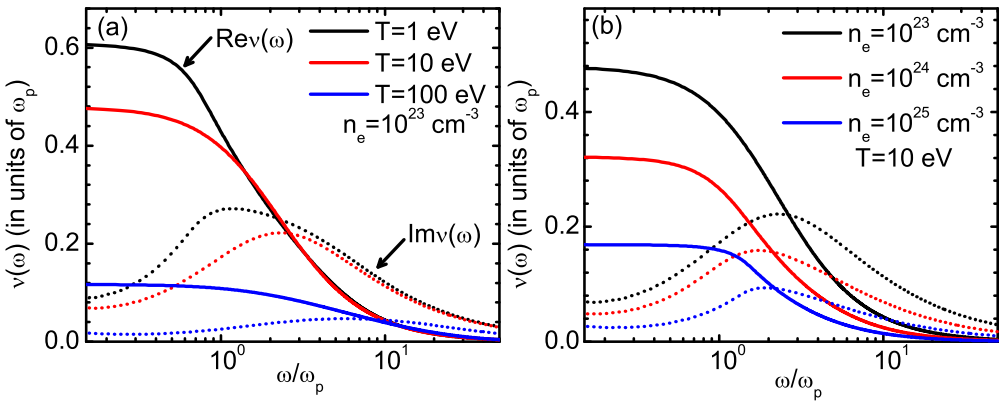


FIG. 2. Real part (solid curves) and imaginary part (dotted curves) of the DCF $\nu(\omega)$ as a function of the frequency $\omega$. (a) is for the Be plasmas with electron density $n_e = 10^{23}$ cm$^{-3}$ and temperatures $T = 1$, 10, and 100 eV, and (b) is for the Be plasmas with temperature $T = 10$ eV and electron densities $n_e = 10^{23}$, $10^{24}$, and $10^{25}$ cm$^{-3}$. Mean ionization degree $\langle Z \rangle$ is considered in all calculations.

part of $\nu(\omega)$ vanishes and the real part of $\nu(\omega)$ tends to the SCF. In the static limit, $\nu_S \equiv \nu(\omega \to 0)$ in Eq. (2) is determined by the generalized static Lenard-Balescu model $\nu_S = \sum_\alpha \nu_{\alpha,S}(\omega = 0)$. Here, $\nu_{\alpha,S}(\omega = 0) = \nu_{\alpha 0} \ln \Lambda_{e\alpha}$, where $\nu_{\alpha 0} = \frac{8m_e^2 q_\alpha^2 e^2}{3\pi\hbar^3 m_\alpha}$, with $q_\alpha$ being the effective charge of component $\alpha$. The Coulomb logarithm $\ln \Lambda_{e\alpha}$ can be obtained by considering the SLFC. For instance, $\ln \Lambda_{ei}$ can be approximated as (for Coulomb scattering) $\ln \Lambda_{ei} = \int_0^\infty dk \frac{1-G_{ei}(k)}{k|\epsilon_e(k,0)|^2} W(k)$, where $W(k) = \{1 + \exp[T(E_{k/2} - \mu)/\mathcal{E}_F^2]\}^{-1}$ and $G_{ei}(k)$ is the $e$-$i$ SLFC [42,43]. Similar expressions could also be obtained via non-Born-approximated treatments for static Coulomb scattering [62].

Now let us turn to discuss the properties of LFC. The short-range correlation effects between particles are taken into account via the LFC. We first perform the self-consistent calculations for the SLFC. For this purpose, we self-consistently solve Eqs. (3) and (B3)–(B5). The numerical simulations need quite a large dynamic range in $k$ in order to describe the full variation of $G_{ee}(k,0)$ and $G_{ii}(k,0)$. The present calculations used $2^{17}$ points in $k$, which should be large enough. In Fig. 3, we exhibit the $e$-$e$ SLFC $G_{ee}(k,0)$ and the ion-ion SLFC $G_{ii}(k,0)$ for WDP of Be at electron density $n_e = 10^{23}$ cm$^{-3}$ and three different values of temperature $T = 10$, 50, and 100 eV. We can see from Fig. 3 that the SLFC $G_{ee}(k,0)$ and $G_{ii}(k,0)$ vanish at low momentum $k$ and increase to unity at high momentum. When the temperature is low, SLFC oscillates out of several times the electron sphere radius $a_e = (3/4\pi n_e)^{1/3}$, while the oscillation phenomena disappear with increasing temperature. For example, the first two peaks of $G_{ii}(k,0)$ are clearly observed when the temperature $T = 10$ eV; see the thin black curve in Fig. 3. The high-frequency limit of DLFC, i.e., $G_{ee}(k,\infty)$ and $G_{ii}(k,\infty)$, is obtained following from the analytical expression (B1). From the above formulas, we see that if one numerically gets the SLFC $G_{\alpha\alpha}(k,0)$, it is easy to get the DLFC via interpolation expressions for $G_{ee}(k,\omega)$ and $G_{ii}(k,\omega)$, such as Eq. (4). Therefore, the results of DLFC will not be shown for the sake of brevity.

Furthermore, the dielectric function $\tilde{\epsilon}_M(k,\omega)$ containing DLFC and the DCF can be easily calculated. The SLFC and the SCF could also be employed in the extended Mermin dielectric function. Although there exist some drawbacks, various studies indicate that the DLFC method is in good agreement with other methods in wide ranges of plasma density and temperature, such as the hydrodynamic model [63] and the moments method [25].

By using Eq. (7), we obtain the stopping power of a proton moving in the WDP of Be with electron density $n_e = 2.78 \times 10^{23}$ cm$^{-3}$ and temperature $T = 40$ eV. The corresponding mean ionization degree $\langle Z \rangle = 2.26$ and chemical potential $\mu = -6.56$ eV are used in the calculations. Figure 4 represents the typical results of stopping power (in units of MeV/$\mu$m) as a function of the velocity of projected proton $v_p$, normalized to the electron thermal velocity $\bar{v}_e = (3T/m_e)^{1/2}$. To clearly show the contributions from the electron component and the ion component, respectively, we display the electron part of the stopping power $dE_{\rm ele}/dx$ in Fig. 4(a), and the ion part of the stopping power $dE_{\rm ion}/dx$ in Fig. 4(b). For comparison, the RPA results are shown; see the black open circles in Fig. 4. The blue squares denote the results obtained from the

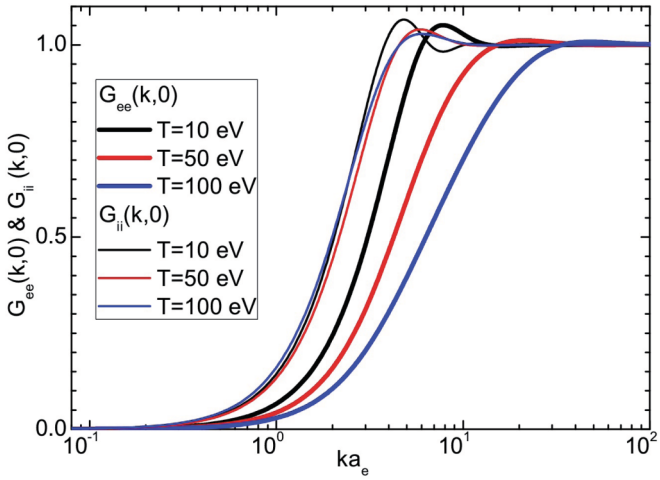


FIG. 3. Electron-electron SLFC $G_{ee}(k,0)$ (thick curves) and ion-ion SLFC $G_{ii}(k,0)$ (thin curves) as a function of the $ka_e$ for Be plasmas at three different temperatures $T = 10$, 50, and 100 eV and electron density $n_e = 10^{23}$ cm$^{-3}$. In the calculations, the mean ionization degree and chemical potential of Be plasma shown in Fig. 1 were used.

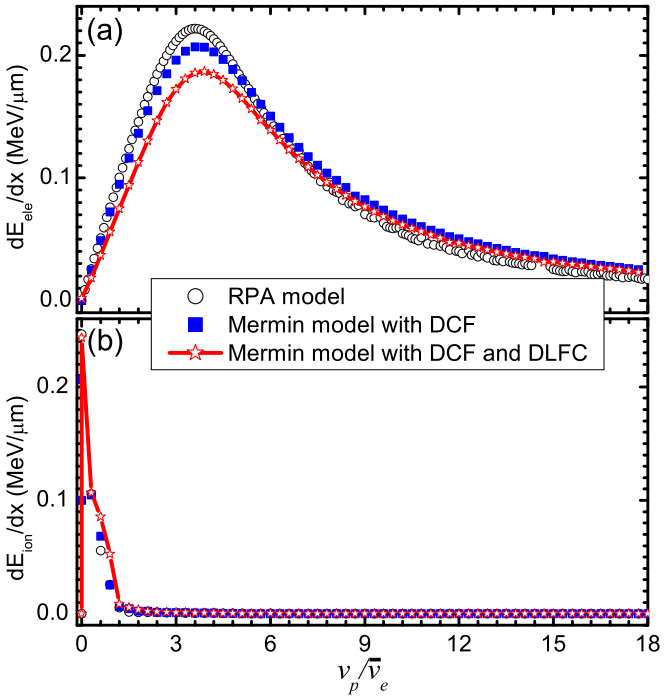


FIG. 4. Proton particle moving the WDP of Be. The stopping power splitting into separate (a) electron component $dE_{\rm ele}/dx$ and (b) ion component $dE_{\rm ion}/dx$ are plotted vs particle velocity $v_p$ (in units of thermal velocity of electron $\bar{v}_e$). Different inverse dielectric function models, including the RPA model (black open circles), the Mermin model with DCF $\nu(\omega)$ (blue solid squares), and the EMDF with both DCF $\nu(\omega)$ and DLFCs $G_{\alpha\alpha}(k,\omega)$ with $\alpha = e,i$ (red open stars) were considered. The temperature of Be plasma is chosen as $T = 40$ eV, and the electron density is $n_e = 2.78 \times 10^{23}$ cm$^{-3}$.

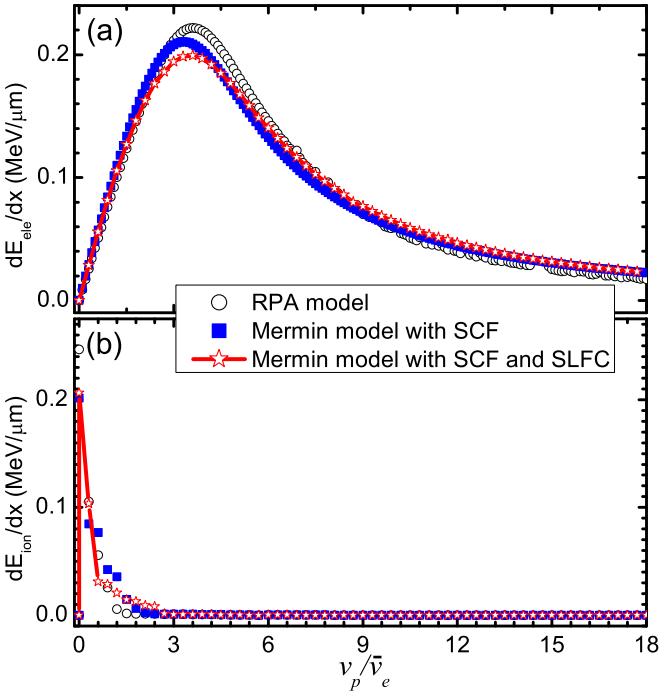


FIG. 5. Same as Fig. 4, but the SCF $\nu_S$ and SLFCs $G_{\alpha\alpha}(k,0)$ with $\alpha = e,i$ were used in the Mermin model and the EMDF model. Other parameters are the same as those in Fig. 4.

Mermin dielectric function model $\epsilon_M(\boldsymbol{k},\omega)$ within the DCF $\nu(\omega)$. Results obtained from the EMDF model $\tilde{\epsilon}_M(\boldsymbol{k},\omega)$ within both the DCF $\nu(\omega)$ and the DLFC $G_{\alpha\alpha}(k,\omega)$ are plotted by the open red stars. Compared with the RPA result for the electron part [see Fig. 4(a)], we observe distinct differences induced by the DCF and the DLFC in the EMDF model. In particular, around the maximum stopping, compared with the RPA result, the difference is significant when the short-range correlation effects are considered for the DLFC in the EMDF model, almost ∼20%. As mentioned above, the Yukawa potential is used in the present calculations of the DLFC, including in the EMDF model. It can be easily reduced to the DLFC of the bare Coulomb interaction [56] by setting the screening length $\kappa_\alpha = 0$. The departure of the EMDF model from the RPA model arises mainly from the DLFC rather than the Yukawa potential taken into account in the model. Another advantage of the Yukawa potential employed herein is the remarkable reduction in the computational amount since the Yukawa potential is a short-range potential.

The EMDF model indicates that a significantly reduced stopping will give rise to a range enhancement for the DLFC. This is important for ICF ignition. In other words, this uncertainty is critical for the prediction of charged-particle heating in fusion plasmas since $v_p \leqslant \bar{v}_e$ holds for most of the deposition range of the charged particle [21,48]. Other transport coefficients and relaxation behaviors of WDP, where the dynamic properties become of importance, may also be remarkably affected. The advanced progress in ion-stopping experiments on the PHELIX laser facility at GSI Helmholtzzentrum für Schwerionenforschung in Darmstadt, Germany [48,64], and the OMEGA laser facility at the University of Rochester, USA [34,35], enables an experimental investigation of the discrepancies of different stopping power models in such a WDP. Thereby, we hope this finding can be tested in future experiments.

At higher velocities, Mermin results tend to the same values of RPA results. For the ion part of the stopping power, the differences between different models is indistinct in our calculations; see Fig. 4(b). The maximum stopping induced by ions is close to zero point of velocity due to the larger mass of the proton with respect to the mass of the electron.

Furthermore, we also calculate the stopping power by the Mermin model within SCF $\nu_S$ and SLFC $G_{\alpha\alpha}(k,0)$. The corresponding results are shown in Fig. 5. The other parameters in this figure are the same as those used in Fig. 4. Differing from the dynamic case, the SCF is no longer a complex function of $\omega$ but just a real value, $\nu_S = 12.8$ fs$^{-1}$, in the calculations. There are at least two points that should be noticed: (i) In the static case, the Mermin stopping power is close to the RPA result; see the blue squares in Fig. 5. The *e*-*e* static collision becomes unimportant for heavier matters, such as Fe, Au, and so on, while it is pronounced in a plasma composed of light elements, such as H, He, Be, and so on [65]. The *e*-*e* SCF produces an enhancement of stopping power before the maximum, but the differences between including or not including the *e*-*e* collision is not clear. This is because the effect of the *e*-*e* collision becomes distinct if the *e*-*e* SCF is compared with the plasma frequency. In the present calculation, $\nu_{ee,S}/\omega_p$ is 0.12.

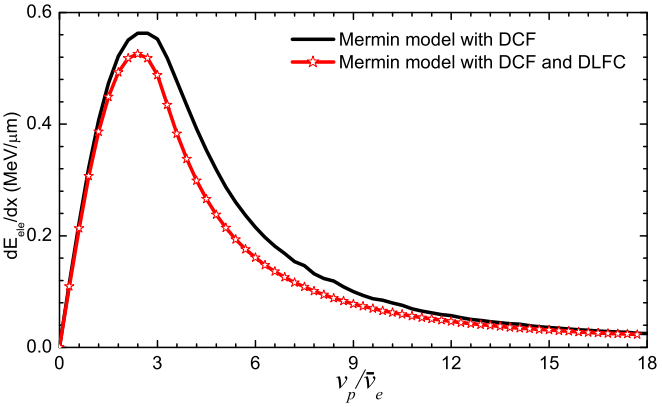


FIG. 6. Stopping power $dE_{\rm ele}/dx$ obtained from the Mermin model (black curve) and the EMDF model (red stars) with DCF $\nu(\omega)$ and DLFC $G_{ee}(k,\omega)$. The temperature of Be plasma is $T = 100$ eV, and the electron density is $n_e = 4 \times 10^{23}$ cm$^{-3}$.

Thereby, the differences induced by $e$-$e$ collisions are weak in the stopping power. (ii) If the SLFC are taken into account in the EMDF model, a departure from the RAP stopping power becomes visible around the maximum value; see the red stars in Fig. 5. This indicates that the short-range correlations between plasma component particles should be considered in the warm dense regime. However, the modification induced by SCF and SLFC is weaker than that induced by the dynamic ones in Fig. 4. Therefore, the dynamic properties in the WDP may be more important and more significant.

Presently, the WDP with electron density around solid values $n_e \sim 10^{23}$ cm$^{-3}$ and temperatures from 10 to 100 eV is interesting for ICF studies. The exact determination of the plasma condition (density and temperature) is still a challenge in the present ICF-related experiments. For example, in Ref. [35] the temperature data are estimated to be 32 eV with a large uncertainty of $\pm 15$ eV, the electron density is around $\sim 10^{23}$ cm$^{-3}$, and the corresponding mean ionization gives $\langle Z \rangle = 2.28^{+0.42}_{-0.27}$, which is consistent with our calculations in Fig. 1. If the temperature is as high as 100 eV, we find $\langle Z \rangle = 3.2$ and $n_e \approx 3.8 \times 10^{23}$ cm$^{-3}$. The electron part of the total stopping power for this plasma condition obtained from the Mermin model and the EMDF model within DCF and DLFC is shown in Fig. 6. It is clear that when the DLFC is introduced into the model, the stopping power is strongly modified at the moderate velocity regime, i.e., $3 < v_p/\bar{v}_e < 9$. At higher velocity, both results tend to agree with the RPA result. In addition, similar to the above Figs. 4(b) and 5(b), the DLFC-induced modification to the ion part of the stopping power is weak under the present plasma conditions. Thus we do not show the corresponding results for the sake of brevity.

To obtain the energy loss, however, one can first obtain the deposition length by integrating the inverse of the stopping power over the energy deposited, $L(E_i, E_f) = -\int_{E_f}^{E_i} \frac{dx}{dE} dE$, where $E_i$ is the initial energy and $E_f$ is the final energy of the particle. For our formulas shown above, we have

$$L(E_i, E_f) = -\int_{E_f}^{E_i} \left[ \frac{dE_{\rm ele}}{dx} + \frac{dE_{\rm ion}}{dx} \right]^{-1} dE, \qquad (8)$$

and $\Delta E = |E_f - E_i|$.

Choosing the experimental condition shown in Ref. [35], i.e., $E_i = 15$ MeV, $L = 532$ $\mu$m, $n_e = 2.78 \times 10^{23}$ cm$^{-3}$, $T = 40$ eV, and $\langle Z \rangle = 2.26$, and using the EMDF model within DCF and DLFC, we estimate that the final energy of a proton passing through the WDP of Be is about $E_f \approx 12.2$ MeV. Thus, the energy loss is $\Delta E_{\rm EMDF} \approx 2.8$ MeV. This result is reasonably consistent with the experimental data as well as the theoretical results reported in Ref. [35]. Within the same parameters, the Mermin model without DLFC yields $\Delta E_{\rm Mermin} \approx 3.1$ MeV, and the RPA model yields $\Delta E_{\rm RPA} \approx 3.13$ MeV, which may overestimate the energy loss. The result of the static EMDF model within SCF and SLFC is close to that of the Mermin model. Furthermore, we also estimate the contribution of the free-electron part of the stopping power via $L(E_i, E_f) = -\int_{E_f}^{E_i} \frac{dx}{dE_{\rm ele}} dE$, and we obtain $\Delta E^{\rm free}_{\rm EMDF} \approx 2.65$ MeV corresponding to the extended one-component Mermin model. Therefore, consistent with the results in Ref. [35], the partial ionization and the dynamic properties are important for the stopping of charged particles moving in the WDP. Different approximations of the DLFC [18,22,24,39,49] may yield different numerical results, but it is clear to us that the DLFC in the presence of EMDF induce an enhancement of energy deposition of charged particles.

Additionally, we also calculate the energy loss by using the BPS stopping power model. According to the BPS method [21], the stopping power of nonrelativistic particles moving through a fully ionized plasma for Coulomb interaction includes three parts: (i) the classical short-distance contribution, (ii) the classical long-distance contribution, and (iii) the quantum correction to the classical part. In the BPS model, the electrons and ions are considered classical particles that obey the Maxwell-Boltzmann distribution. We find that, for a fully ionized plasma, $\Delta E_{\rm BPS} \approx 1.6$ MeV if all three parts are included in the calculations, and $\Delta E^{c}_{\rm BPS} \approx 3.5$ MeV if the quantum correction to the classical part is not considered in the calculations. These results are far from the experimental data and the EMDF result, which indicates that the BPS model is not suitable for the WDP. This is because that BPS model is only suitable for the weakly coupled plasmas, while the WDP of Be considered herein is located at the moderate coupling regime, i.e., $\Gamma_e = \frac{e^2}{(3/4\pi n_e)^{1/3} T} \approx 0.3$. However, the EMDF model is suitable for plasma systems in a wide coupling range and any degeneracy. Finally, we point out that the EMDF model including the DCF and DLFC also agrees with other models, such as the average-atom local density approximation model [16,17,20,23], the moments method [25], the full-conserving dielectric function model [66], and so on. Therefore, our results shown in this work should be reasonable.

## IV. CONCLUSION

In this paper, we have studied theoretically the energy loss of multi-MeV charged particles traveling in the WDP with degenerate electrons and nondegenerate ions. The mean ionization degree has been considered by the detailed configuration accounting model and the average-atom model. The stopping power model we employed is based on the plasma dielectric functions. We focused on the dynamic properties of the stopping of a proton moving in the plasmas. Therefore,

beyond the RPA model, the short-range correlations between plasma component particles are taken into account by DLFC in an EMDF for two-component plasmas. The Yukawa-type effective potential has also been employed to derive the DLFC. The DLFC were obtained by numerically self-consistent iterative calculations. Our results show that, compared with the RPA result, the DLFC introduced in the EMDF model give rise to a significant difference around the maximum stopping, almost 20%. However, the modification by the SLFC is weak enough to be ignored. As part of the progress of the advanced laser facilities, these uncertainties between different models may be tested experimentally in the future. Furthermore, by using the two-component EMDF within DLFC, we have estimated the energy loss of a proton with an initial energy of $E_i = 15$ MeV passing through a WDP of Be with solid density and temperature around $T = 40$ eV. The numerical result is reasonably consistent with the experimental data [35]. The results in this work indicate that the partial ionization and the dynamic properties are important for the stopping of charged particles moving in the WDP.

## ACKNOWLEDGMENTS

This work was supported by the Science Challenge Project (Grant No. JCKY201612A501), by the President Foundation of China Academy of Engineering Physics (CAEP) under Grant No. YZ2015014, by the Foundation for the Development of Science and Technology of CAEP under Grants No. 2014B0102015 and No. 2015B0102022, by National Natural Science Foundation of China under Grants No. 11675023, No. 11675024, No. 11575032, No. 11304009, No. 11205019, and No. U1530258, and by the National Magnetic Confinement Fusion Energy Research Project of China under Grant No. 2015B108002. Z.-G.F. was also partially supported by the China Postdoctoral Science Foundation under Grant No. 2014T70029. We thank Bin He for useful discussions.

## APPENDIX A: DERIVATIONS FOR THE RPA DIELECTRIC FUNCTION

The dielectric function model under the RPA [12] is given by

$$\epsilon_e(\boldsymbol{k},\omega) = 1 + \frac{V(\boldsymbol{k})}{4\pi^3}\int d\boldsymbol{q}\,\frac{f(\boldsymbol{k}+\boldsymbol{q}) - f(\boldsymbol{q})}{\hbar\omega - (E_{\boldsymbol{k}+\boldsymbol{q}} - E_{\boldsymbol{q}})}, \quad \text{(A1)}$$

where $V(\boldsymbol{k})$ denotes the Fourier transform of the interaction potential, $E_{\boldsymbol{k}} = \hbar^2k^2/2m_e$ is the kinetic energy of electrons, with $m_e$ the electron mass and $\hbar$ the Planck constant, and $f(\boldsymbol{k}) = \{1 + \exp[(E_{\boldsymbol{k}} - \mu)/T]\}^{-1}$ represents the Fermi distribution function, with $\mu$ being the chemical potential of plasma and $T$ the temperature (in units of eV) of the system. Considering the Yukawa effective interaction potential $V_{ee}(r) = \frac{e^2}{r}e^{-\kappa_e r}$, with $\kappa_e$ the electronic inverse screening length, the RPA dielectric function for the free electrons can be derived as

$$\epsilon_e(\boldsymbol{k},\omega) = 1 + \frac{2k_F^2}{\pi a_B k\left(k^2+\kappa_e^2\right)}[g(\alpha_+) - g(\alpha_-)], \quad \text{(A2)}$$

where $k_F = (3\pi^2 n_e)^{1/3}$ is the Fermi wave vector, $a_B = \hbar^2/m_e e^2$ is the Bohr radius, and $g(\alpha_\pm) = \int \frac{x\,dx}{\exp[(x^2\mathcal{E}_F - \mu)/T]+1}\ln\frac{\alpha_\pm + x}{\alpha_\pm - x}$, with $\mathcal{E}_F$ being the Fermi energy, and $\alpha_\pm = \frac{\omega + i\nu(\omega)}{kv_F} \pm \frac{k}{2k_F}$, with $v_F = \hbar k_F/m_e$ being the Fermi velocity. The classical RPA dielectric function for ions is written as

$$\epsilon_i(\boldsymbol{k},\omega) = 1 + A(k)\left[1 + \frac{\omega}{k\bar{v}_i}\varphi(z)\right]. \quad \text{(A3)}$$

Here, $\bar{v}_i = (3T/m_i)^{1/2}$ is the thermal velocity of ions, with $m_i$ the ion mass, and $\varphi(z) = \int_{-\infty}^{+\infty}\frac{ds}{\sqrt{\pi}}\frac{se^{-s^2/2}}{s-z}$, where $z = \omega/k\bar{v}_i$. $A(k) = \frac{V_{ii}(k)q_{Di}^2}{4\pi\langle Z\rangle^2 e^2}$, where $V_{ii}(k) = \frac{4\pi\langle Z\rangle e^2}{k^2+\kappa_i^2}$ with $\kappa_i$ the ionic inverse Yukawa screening length, and $q_{Di}^2 = 4\pi n_i\langle Z\rangle^2 e^2/T$ is the Debye screening wave vector, with $\langle Z\rangle$ the mean ionization degree and $n_i = n_e/\langle Z\rangle$ the ion density.

## APPENDIX B: SLFC $G_{\alpha\alpha}(k,\infty)$ AND $G_{\alpha\alpha}(k,0)$

In the derivations of the DLFC, the Yukawa potential [50–54] $V_{\alpha\alpha}(r) = \frac{(Z_\alpha e)^2}{r}e^{-\kappa_\alpha r}$, where $\kappa_\alpha$ is the inverse screening length, is employed to describe the effective interaction potential between plasma species. The Yukawa potential is considered as a screened Coulomb potential. The Yukawa screening length reduces to either the Debye-Huckel law or the Thomas-Fermi distance in the limiting cases of classical and degenerate electron fluid, respectively [51]. For $\kappa_\alpha = 0$, one recovers the bare Coulomb interaction potential model. If a bare Coulomb interaction potential is used in the theoretical model, the effects of bound electrons may be neglected, and thus the bare Coulomb interaction model may yield insufficient information on dynamic properties (such as DLFC and dynamic structure factors) for most warm dense matter systems created experimentally. To describe appropriately the warm dense matter, we must consider the quantum behavior of the electrons and strong interactions between the plasma species. Based on these considerations, the Yukawa potential approximation may be a good choice for the derivation of DLFC. By using the recurrence-relation technique and considering the Yukawa effective interaction potential $V_{\alpha\alpha}(k)$, the lowest dynamical extension of the DLFC could be introduced [49]. One can get the high-frequency limit of DLFC as follows:

$$G_{\alpha\alpha}(k,\infty) = \frac{V_{\alpha\alpha}^0(k)}{n_\alpha V_{\alpha\alpha}(k)}\int_0^\infty dq\,q^2[1 - S_{\alpha\alpha}(q)]h_\alpha(q,k), \quad \text{(B1)}$$

where $V_{\alpha\alpha}^0(k)$ is the pure Coulomb potential of species $\alpha$, and $S_{\alpha\alpha}(q)$ is the static structure factors for species $\alpha$. The form factor $h_\alpha(q,k)$ in Eq. (B1) is written as

$$h_\alpha(q,k) = \frac{1}{8\pi^2}\left[3 - \frac{(2a_qa_k)^2 - 3\left(a_q^2+1\right)^2}{3a_k^2\left(a_q^2+1\right)} + \frac{\left(a_q^2 - a_k^2 + 1\right)^2}{4a_k^3a_q} \times \ln\frac{(a_q+a_k)^2+1}{(a_q-a_k)^2+1}\right], \quad \text{(B2)}$$

with $a_q = q/\kappa_\alpha$ and $a_k = k/\kappa_\alpha$. This expression (B1) is a generalization of the SLFC developed by Pathak and Vashista [56]. Our formulas could be easily reduced to the case of

the bare Coulomb interaction, which has been developed by Pathak and Vashista [56]. The SLFC at $\omega = 0$ used in our formulas is obtained by self-consistently solving the following equations [67]:

$$G_{ee}(k,0) = \frac{1}{n_e}\int \frac{d^3q}{(2\pi)^3}\frac{\boldsymbol{q}\cdot\boldsymbol{k}}{q^2}[1 - S_{ee}(\boldsymbol{k}-\boldsymbol{q})], \tag{B3}$$

$$S_{ee}(\boldsymbol{k}) = \frac{1}{n_e V_{ee}(\boldsymbol{k})}\int_0^\infty \frac{d\omega}{\pi}\frac{\mathrm{Im}\,[\epsilon_e(\boldsymbol{k},\omega)]^{-1}}{e^{-\hbar\omega/T}-1}. \tag{B4}$$

Furthermore, the ion-ion SLFC can be derived as the following form:

$$G_{ii}(k,0) = \frac{1}{\epsilon_e(k,0)} - \frac{T}{n_i V_{ii}(k)}\left[\frac{1}{S_{ii}(k)} - 1\right]. \tag{B5}$$

In addition, the SLFC could also be obtained by self-consistently solving the Ornstein-Zernike (OZ) equations in Fourier space and the correlated hypernetted-chain closure (HNC) in real space [42,43]. Substituting Eqs. (B1)–(B5) into Eq. (4), one can easily get the DLFC.

## APPENDIX C: HIGH-FREQUENCY LIMIT OF DCF

Moreover, the high-frequency limit of the RPA dielectric function for electrons (A2) is presented as

$$\epsilon_e(\boldsymbol{k},\omega\to\infty) = 1 - \frac{\omega_p^2}{\omega^2} - \frac{\omega_p^4\gamma(k)}{\omega^4} - \cdots, \tag{C1}$$

where

$$\gamma(k) = \frac{3F_{3/2}(\eta)}{m_e T^{-5/2}\mathcal{E}_F^{3/2}}\frac{k^2}{\omega_p^2} + \frac{\hbar^2}{4m_e^2}\frac{k^4}{\omega_p^2}. \tag{C2}$$

Here, we have used the relation

$$g(\alpha_\pm\to\infty) = \sum_{\delta=1,3,5,\ldots}\frac{F_{\delta/2}(\eta)}{\delta\alpha_\pm^\delta(\mathcal{E}_F/T)^{\delta/2+1}}. \tag{C3}$$

Similarly, the RPA ionic classical dielectric function can be reduced to

$$\epsilon_i(k,\omega\to\infty) = 1 - \frac{\omega_{ip}^2}{\omega^2} - \frac{3Tk^2}{m_i}\frac{\omega_{ip}^2}{\omega^4} - \frac{15T^2k^4}{m_i^2}\frac{\omega_{ip}^2}{\omega^6} - \cdots, \tag{C4}$$

where $\omega_{ip} = (\langle Z\rangle m_e/m_i)^{1/2}\omega_p$ is the ionic plasma frequency. As a consequence, in the high-frequency limit $\omega\to\infty$, the real part of $\nu(\omega)$ vanishes and the DCF is approximated as a pure imaginary one, so that

$$\nu(\omega\to\infty) = i\left(\frac{\nu_1}{\omega} + \frac{\nu_3}{\omega^3} + \frac{\nu_5}{\omega^5} + \cdots\right), \tag{C5}$$

where

$$\nu_1 = \frac{1}{\omega_{ep}^2}\int_0^\infty dk\,U(k)[\epsilon_e(k,0) - 1], \tag{C6}$$

$$\nu_3 = \int_0^\infty dk\,U(k), \tag{C7}$$

$$\nu_5 = \omega_{ep}^2\int_0^\infty dk\,U(k)\gamma(k), \tag{C8}$$

with $U(k) = \frac{n_i}{6\pi^2 m_e^2}k^6 V_{ei}^2(k)S_{ii}(k)$.


[1] J. D. Lindl, P. Amendt, R. L. Berger, S. G. Glendinning, S. H. Glenzer, S. W. Haan, R. L. Kauffman, O. L. Landen, and L. J. Suter, The physics basis for ignition using indirect-drive targets on the National Ignition Facility, Phys. Plasmas **11**, 339 (2004).

[2] S. Atzeni and J. Meyer-ter-Vehn, *The Physics of Inertial Fusion: Beam Plasma Interaction, Hydrodynamics, Hot Dense Matter*, International Series of Monographs on Physics (Clarendon, Oxford, 2004).

[3] S. H. Glenzer, B. J. MacGowan, P. Michel, N. B. Meezan, L. J. Suter, S. N. Dixit, J. L. Kline, G. A. Kyrala, D. K. Bradley, D. A. Callahan *et al.*, Symmetric inertial confinement fusion implosions at ultra-high laser energies, Science **327**, 1228 (2010).

[4] C. K. Li, F. H. Séguin, J. A. Frenje, M. Rosenberg, R. D. Petrasso, P. A. Amendt, J. A. Koch, O. L. Landen, H. S. Park, H. F. Robey *et al.*, Charged-particle probing of x-ray-driven inertial-fusion implosions, Science **327**, 1231 (2010).

[5] O. A. Hurricane, D. A. Callahan, D. T. Casey, P. M. Celliers, C. Cerjan, E. L. Dewald, T. R. Dittrich, T. Döppner, D. E. Hinkel, L. F. Berzak Hopkins *et al.*, Fuel gain exceeding unity in an inertially confined fusion implosion, Nature **506**, 343 (2014).

[6] W. Theobald, A. A. Solodov, C. Stoeckl, K. S. Anderson, F. N. Beg, R. Epstein, G. Fiksel, E. M. Giraldez, V. Yu. Glebov, H. Habara *et al.*, Time-resolved compression of a capsule with a cone to high density for fast-ignition laser fusion, Nat. Commun. **5**, 5785 (2014).

[7] R. K. Follett, J. A. Delettrez, D. H. Edgell, V. N. Goncharov, R. J. Henchen, J. Katz, D. T. Michel, J. F. Myatt, J. Shaw, A. A. Solodov *et al.*, Two-Plasmon Decay Mitigation in Direct-Drive Inertial-Confinement-Fusion Experiments Using Multilayer Targets, Phys. Rev. Lett. **116**, 155002 (2016).

[8] D. Turnbull, P. Michel, T. Chapman, E. Tubman, B. B. Pollock, C. Y. Chen, C. Goyon, J. S. Ross, L. Divol, N. Woolsey, and J. D. Moody, High Power Dynamic Polarization Control Using Plasma Photonics, Phys. Rev. Lett. **116**, 205001 (2016).

[9] F. Wagner, O. Deppert, C. Brabetz, P. Fiala, A. Kleinschmidt, P. Poth, V. A. Schanz, A. Tebartz, B. Zielbauer, M. Roth *et al.*, Maximum Proton Energy Above 85 MeV from the Relativistic Interaction of Laser Pulses with Micrometer Thick $CH_2$ Targets, Phys. Rev. Lett. **116**, 205002 (2016).

[10] N. Bohr, On the theory of the decrease of velocity of moving electrified particles on passing through matter, Philos. Mag. **25**, 10 (1913).

[11] H. Bethe, Zur theorie des durchgangs schneller korpuskularstrahlen durch materie, Ann. Phys. (Leipzig) **397**, 325 (1930); F. Bloch, Zur bremsung rasch bewegter teilchen beim durchgang durch materie, *ibid.* **408**, 285 (1933).

[12] J. Lindhard, On the properties of a gas of charged particles, Kgl. Danske Videnskab. Selskab Mat.-Fys. Medd. **28**, 8 (1954).

[13] D. O. Gericke and M. Schlanges, Beam-plasma coupling effects on the stopping power of dense plasmas, Phys. Rev. E **60**, 904 (1999).
[14] B. Trubnikov, *Particle Interactions in a Fully Ionized Plasma* (Consultant's Bureau, New York, 1965).
[15] N. D. Mermin, Lindhard dielectric function in the relaxation-time approximation, Phys. Rev. B **1**, 2362 (1970).
[16] G. Maynard and C. Deutsch, Energy loss and straggling of ions with any velocity in dense plasmas at any temperature, Phys. Rev. A **26**, 665 (1982).
[17] G. Zimmerman, LLNL Report No. UCRL-JC-105616 (1990).
[18] S. Ichimaru, *Statistical Plasma Physics, Vol. I: Basic Principles* (Addison-Wesley, Reading, MA, 1992).
[19] C. K. Li and R. D. Petrasso, Charged-Particle Stopping Powers in Inertial Confinement Fusion Plasmas, Phys. Rev. Lett. **70**, 3059 (1993); Erratum: Charged-Particle Stopping Powers in Inertial Confinement Fusion Plasmas, *ibid.* **114**, 199901 (2015).
[20] I. Nagy and B. Apagyi, Scattering-theory formulation of stopping powers of a solid target for protons and antiprotons with velocity-dependent screening, Phys. Rev. A **58**, R1653 (1998).
[21] L. S. Brown, D. L. Preston, and R. L. Singleton, Jr., Charged particle motion in a highly ionized plasma, Phys. Rep. **410**, 237 (2005).
[22] A. Wierling, Dynamic local field corrections for two-component plasmas at intermediate coupling, J. Phys. A **42**, 214051 (2009).
[23] G. Faussurier, C. Blancard, P. Cossé, and P. Renaudin, Equation of state, transport coefficients, and stopping power of dense plasmas from the average-atom model self-consistent approach for astrophysical and laboratory plasmas, Phys. Plasmas **17**, 052707 (2010).
[24] C. Fortmann, A. Wierlingm, and G. Ropke, Influence of local-field corrections on Thomson scattering in collision-dominated two-component plasmas, Phys. Rev. E **81**, 026405 (2010).
[25] Yu. V. Arkhipov, A. B. Ashikbayeva, A. Askaruly, A. E. Davletov, and I. M. Tkachenko, Dielectric function of dense plasmas, their stopping power, and sum rules, Phys. Rev. E **90**, 053102 (2014).
[26] P. E. Grabowski, M. P. Surh, D. F. Richards, F. R. Graziani, and M. S. Murillo, Molecular Dynamics Simulations of Classical Stopping Power, Phys. Rev. Lett. **111**, 215002 (2013).
[27] R. L. Liboff, *Kinetic Theory: Classical, Quantum, and Relativistic Descriptions, Graduate Texts in Contemporary Physics* (Springer, New York, 2003).
[28] J. Ziegler, J. Biersack, and U. Littmark, *The Stopping and Range of Ions in Matter* (Pergamon, New York, 1985).
[29] P. Sigmund, R. Bimbot, H. Geissel, H. Paul, and A. Schinner, *Stopping of Ions Heavier than Helium*, ICRU Report Vol. 73 (Oxford University Press, Oxford, 2005).
[30] H. Paul, A comparison of recent stopping power tables for light and medium-heavy ions with experimental data, and applications to radiotherapy dosimetry, Nucl. Instrum. Methods Phys. Res., Sect. B **247**, 166 (2006).
[31] J. F. Ziegler, M. D. Ziegler, and J. P. Biersack, SRIM—The stopping and range of ions in matter, Nucl. Instrum. Methods Phys. Res., Sect. B **268**, 1818 (2010).
[32] V. U. Nazarov, J. M. Pitarke, C. S. Kim, and Y. Takada, Time-dependent density-functional theory for the stopping power of an interacting electron gas for slow ions, Phys. Rev. B **71**, 121106(R) (2005).
[33] V. U. Nazarov, J. M. Pitarke, Y. Takada, G. Vignale, and Y.-C. Chang, Including nonlocality in the exchange-correlation kernel from time-dependent current density functional theory: Application to the stopping power of electron liquids, Phys. Rev. B **76**, 205103 (2007).
[34] J. A. Frenje, P. E. Grabowski, C. K. Li, F. H. Séguin, A. B. Zylstra, M. Gatu Johnson, R. D. Petrasso, V. Yu. Glebov, and T. C. Sangster, Measurements of Ion Stopping Around the Bragg Peak in High-Energy-Density Plasmas, Phys. Rev. Lett. **115**, 205001 (2015).
[35] A. B. Zylstra, J. A. Frenje, P. E. Grabowski, C. K. Li, G. W. Collins, P. Fitzsimmons, S. Glenzer, F. Graziani, S. B. Hansen, S. X. Hu *et al.*, Measurement of Charged-Particle Stopping in Warm Dense Plasma, Phys. Rev. Lett. **114**, 215002 (2015).
[36] S. B. Hansen, A. Y. Faenov, T. A. Pikuz, K. B. Fournier, R. Shepherd, H. Chen, K. Widmann, S. C. Wilks, Y. Ping, and H. K. Chung *et al.*, Temperature determination using $K\alpha$ spectra from *M*-shell Ti ions, Phys. Rev. E **72**, 036408 (2005).
[37] J. Yan and Z.-Q. Wu, Theoretical investigation of the increase in the Rosseland mean opacity for hot dense mixtures, Phys. Rev. E **65**, 066401 (2002).
[38] S. Vinko, O. Ciricosta, and J. Wark, Density functional theory calculations of continuum lowering in strongly coupled plasmas, Nat. Commun. **5**, 3533 (2014).
[39] M. D. Barriga-Carrasco, Dynamical local field corrections on energy loss in plasmas of all degeneracies, Phys. Rev. E **79**, 027401 (2009).
[40] Yu. V. Arkhipov, A. Askaruly, D. Ballester, A. E. Davletov, I. M. Tkachenko, and G. Zwicknagel, Dynamic properties of one-component strongly coupled plasmas: The sum-rule approach, Phys. Rev. E **81**, 026402 (2010).
[41] G. Faussurier and C. Blancard, Temperature relaxation in dense plasmas, Phys. Rev. E **93**, 023204 (2016).
[42] J. Daligault and G. Dimonte, Correlation effects on the temperature-relaxation rates in dense plasmas, Phys. Rev. E **79**, 056403 (2009).
[43] Z.-G. Fu, Z. Wang, D.-F. Li, W. Kang, and P. Zhang, Generalized Lenard-Balescu calculations of electron-ion temperature relaxation in beryllium plasma, Phys. Rev. E **92**, 033103 (2015).
[44] C. Wang, Y. Long, M.-F. Tian, X.-T. He, and P. Zhang, Equations of state and transport properties of warm dense beryllium: A quantum molecular dynamics study, Phys. Rev. E **87**, 043105 (2013).
[45] J. Kim, B. Qiao, C. McGuffey, M. S. Wei, P. E. Grabowski, and F. N. Beg, Self-Consistent Simulation of Transport and Energy Deposition of Intense Laser-Accelerated Proton Beams in Solid-Density Matter, Phys. Rev. Lett. **115**, 054801 (2015).
[46] G. Röpke, A. Selchow, A. Wieling, and H. Reinholz, Lindhard dielectric function in the relaxation-time approximation and generalized linear response theory, Phys. Lett. A **260**, 365 (1999).
[47] C. Deutsch, N. A. Tahir, M. Barriga-Carrasco, V. Ceban, P. Fromy, D. Gilles, D. Leger, G. Maynard, B. Tashev, and L. Volpe, Multiple scattering in electron fluid and energy loss in multi-ionic targets, Nucl. Instrum. Methods Phys. Res., Sect. A **733**, 39 (2014).
[48] W. Cayzac, V. Bagnoud, M. M. Basko, A. Blazević, A. Frank, D. O. Gericke, L. Hallo, G. Malka, A. Ortner, An. Tauschwitz, J. Vorberger, and M. Roth, Predictions for the energy loss of light

ions in laser-generated plasmas at low and medium velocities, Phys. Rev. E **92**, 053109 (2015).
[49] J. Hong and M. H. Lee, Exact Dynamically Convergent Calculations of the Frequency-Dependent Density Response Function, Phys. Rev. Lett. **55**, 2375 (1985).
[50] S. A. Khrapak, A. V. Ivlev, and G. E. Morfill, Momentum transfer in complex plasmas, Phys. Rev. E **70**, 056405 (2004).
[51] J. P. Mithen, J. Daligault, and G. Gregori, Extent of validity of the hydrodynamic description of ions in dense plasmas, Phys. Rev. E **83**, 015401(R) (2011).
[52] G. J. Kalman, Z. Donkó, P. Hartmann, and K. I. Golden, Strong Coupling Effects in Binary Yukawa Systems, Phys. Rev. Lett. **107**, 175003 (2011).
[53] J. Vorberger, Z. Donko, I. M. Tkachenko, and D. O. Gericke, Dynamic Ion Structure Factor of Warm Dense Matter, Phys. Rev. Lett. **109**, 225001 (2012).
[54] K. N. Dzhumagulova, R. U. Masheyeva, T. Ott, P. Hartmann, T. S. Ramazanov, M. Bonitz, and Z. Donkó, Cage correlation and diffusion in strongly coupled three-dimensional Yukawa systems in magnetic fields, Phys. Rev. E **93**, 063209 (2016).
[55] K. Morawetz and G. Röpke, Stopping power in nonideal and strongly coupled plasmas, Phys. Rev. E **54**, 4134 (1996).
[56] K. N. Pathak and P. Vashishta, Electron correlations and moment sum rules, Phys. Rev. B **7**, 3649 (1973).
[57] G. Zwicknagel, C. Toepffer, and P.-G. Reinhard, Stopping of heavy ions in plasmas at strong coupling, Phys. Rep. **309**, 117 (1999).
[58] G. Zwicknagel, Nonlinear energy loss of heavy ions in plasma, Nucl. Instrum. Methods Phys. Res., Sect. B **197**, 22 (2002).
[59] L.-J. Hou, Z. L. Mišković, K. Jiang, and Y.-N. Wang, Energy Loss of a Charged Particle Moving Over a 2D Strongly Coupled Dusty Plasma, Phys. Rev. Lett. **96**, 255005 (2006).
[60] K. Jiang, L.-J. Hou, Y.-N. Wang, and Z. L. Mišković, Excitation of Mach cones and energy dissipation by charged particles moving over two-dimensional strongly coupled dusty plasmas, Phys. Rev. E **73**, 016404 (2006).
[61] L.-J. Hou and Z. L. Mišković, Image force on a charged projectile moving over a two-dimensional strongly coupled Yukawa system, Phys. Rev. E **77**, 046401 (2008).
[62] P. S. Shternin and D. G. Yakovlev, Electron thermal conductivity owing to collisions between degenerate electrons, Phys. Rev. D **74**, 043004 (2006).
[63] P. K. Shukla and M. Akbari-Moghanjoughi, Hydrodynamic theory for ion structure and stopping power in quantum plasmas, Phys. Rev. E **87**, 043106 (2013).
[64] A. Frank, A. Blažević, V. Bagnoud, M. M. Basko, M. Börner, W. Cayzac, D. Kraus, T. Heßing, D. H. H. Hoffmann, A. Ortner *et al.*, Energy Loss and Charge Transfer of Argon in a Laser-Generated Carbon Plasma, Phys. Rev. Lett. **110**, 115001 (2013).
[65] M. D. Barriga-Carrasco, Target electron collision effects on energy loss straggling of protons in an electron gas at any degeneracy, Phys. Plasmas **15**, 033103 (2008).
[66] M. D. Barriga-Carrasco, Proton stopping using a full conserving dielectric function in plasmas at any degeneracy, Phys. Rev. E **82**, 046403 (2010).
[67] G. D. Mahan, *Many-Particle Physics*, 3rd ed. (Kluwer Academic, New York, 2000).